Electronic Supplementary Material (ESI) for Journal of Materials Chemistry C.

Crystal-Field Regulation Enables Broadband-to-Line Emission Switching in Cr^{3+}-Activated Pyroxenes

Yingying Ma,[a] Ting Wen,*[a] Ke Liu,[a] Chen Li,[a] Dequan Jiang,[b] En Chen,[a] Tianyao Pei,[a] Chuanlong Lin,[a] and Yonggang Wang*[b,a]

[a]*Center for High Pressure Science and Technology Advanced Research (HPSTAR), Beijing 100193, China*

[b]*School of Materials Science and Engineering, Peking University, Beijing 100871, China*

*E-mail: ting.wen@hpstar.ac.cn

*E-mail: ygw@pku.edu.cn

Figure S1. PL spectra of (a, b) $LiScSi_2O_6$:0.04Cr^{3+} and (d, e) $LiScGe_2O_6$:0.04Cr^{3+} under compression and decompression. The intensity of $^2E \rightarrow {}^4A_2$ transition under HP, $^4T_2 \rightarrow {}^4A_2$ transition at 0.3 GPa and after release of (c) $LiScSi_2O_6$:0.04Cr^{3+} and (f) $LiScGe_2O_6$:0.04Cr^{3+}. The pressure-dependent $^2E \rightarrow {}^4A_2$ transition of (g) $LiScSi_2O_6$:0.04Cr^{3+}, (h) $LiScGe_2O_6$:0.04Cr^{3+} (i) ruby under HP. (j) The comparative analysis of PL spectra of $LiScSi_2O_6$:0.04Cr^3, $LiScGe_2O_6$:0.04Cr^{3+} and ruby at 16.0 GPa and 22.0 GPa.

Figure S2. Diagram of the bond lengths and bond angles of ScO_6 in (a) *C*2/*c* and (b) $P2_1/c$ phases. The calculated Sc-O distances and O-Sc-O angles as a function of pressure in (c, d) $LiScSi_2O_6$ and (e, f) $LiScGe_2O_6$.

Figure S3. Partial enlargements of (a) *in situ* HP XRD pattern and (b) Lattice volume of $LiScSi_2O_6$. β angle of (c) $LiScSi_2O_6$ and (d) $LiScGe_2O_6$ as a function of pressure.

Figure S4. LeBail fitting results of (a) $LiScSi_2O_6$ at 0.4 GPa, 3.0 GPa, 24.1 GPa and (b) $LiScGe_2O_6$ at 1.1 GPa, 20.3 GPa.

Figure S5. PL spectra of (a) $LiScSi_2O_6$:0.02Eu^{3+} and (b) $LiScGe_2O_6$:0.02Eu^{3+} measured at 80 K and 300 K.

Figure S6. Crystal structures of (a) $LiScSi_2O_6$ and (b) $LiScGe_2O_6$. The twist angles of (c) SiO_4 tetrahedra chains in $LiScSi_2O_6$ and (d) GeO_4 tetrahedra chains in $LiScGe_2O_6$.

Table S1. Energy level transition and crystal field strength (D_q/B) of Some Cr^{3+} activated Phosphors at ambient conditions.

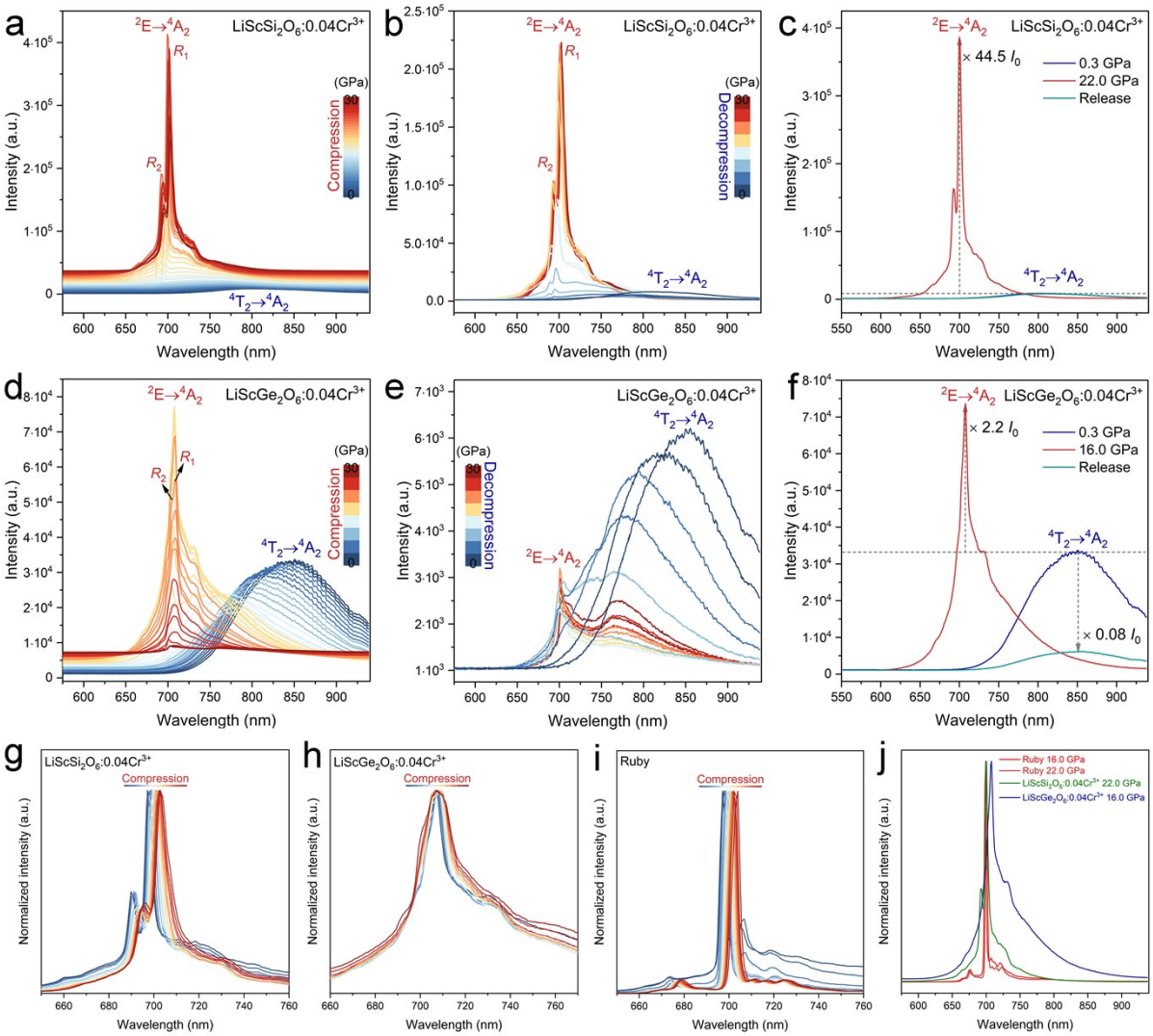

Figure S1. PL spectra of (a, b) $LiScSi_2O_6:0.04Cr^{3+}$ and (d, e) $LiScGe_2O_6:0.04Cr^{3+}$ under compression and decompression. The intensity of $^2E\rightarrow{}^4A_2$ transition under HP, $^4T_2\rightarrow{}^4A_2$ transition at 0.3 GPa and after release of (c) $LiScSi_2O_6:0.04Cr^{3+}$ and (f) $LiScGe_2O_6:0.04Cr^{3+}$. The pressure-dependent $^2E\rightarrow{}^4A_2$ transition of (g) $LiScSi_2O_6:0.04Cr^{3+}$, (h) $LiScGe_2O_6:0.04Cr^{3+}$ (i) ruby under HP. (j) The comparative analysis of PL spectra of $LiScSi_2O_6:0.04Cr^3$, $LiScGe_2O_6:0.04Cr^{3+}$ and ruby at 16.0 GPa and 22.0 GPa.

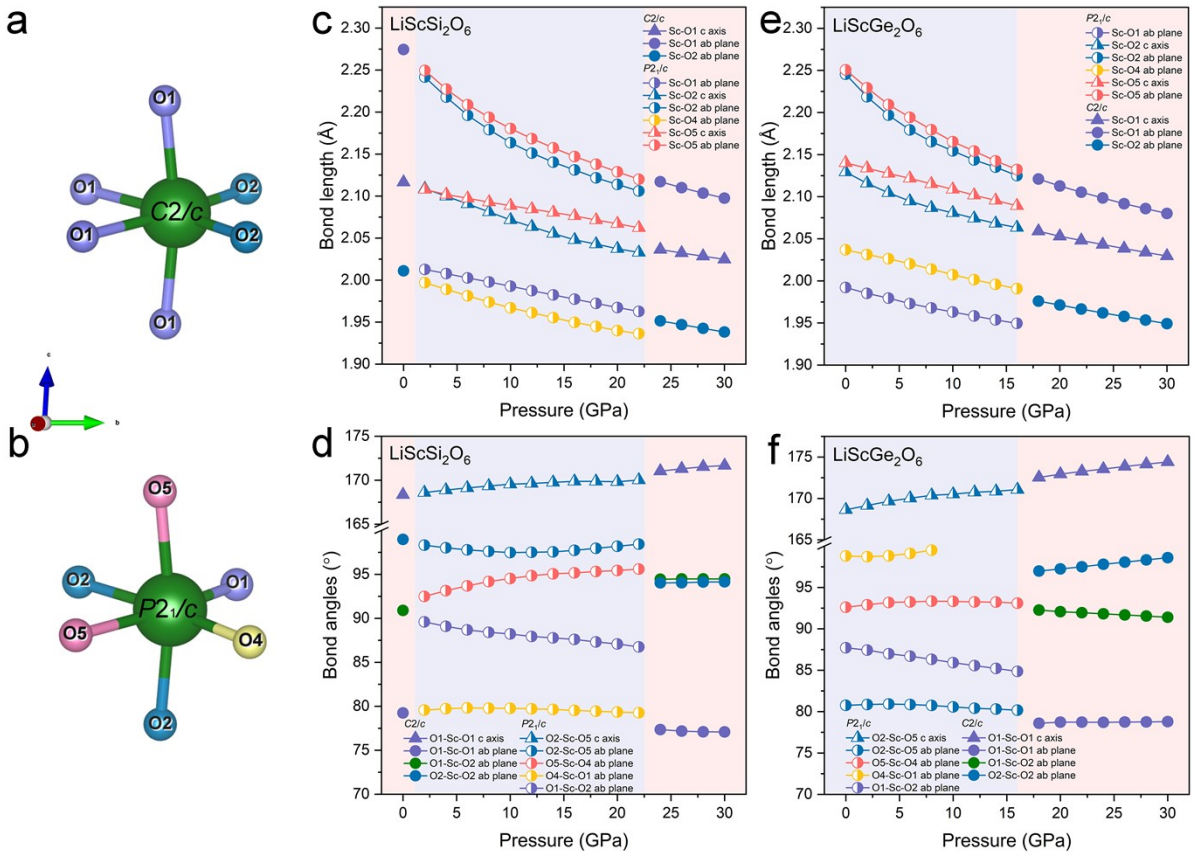

Figure S2. Diagram of the bond lengths and bond angles of ScO_6 in (a) *C*2/*c* and (b) *P*2$_1$/*c* phases. The calculated Sc-O distances and O-Sc-O angles as a function of pressure in (c, d) $LiScSi_2O_6$ and (e, f) $LiScGe_2O_6$.

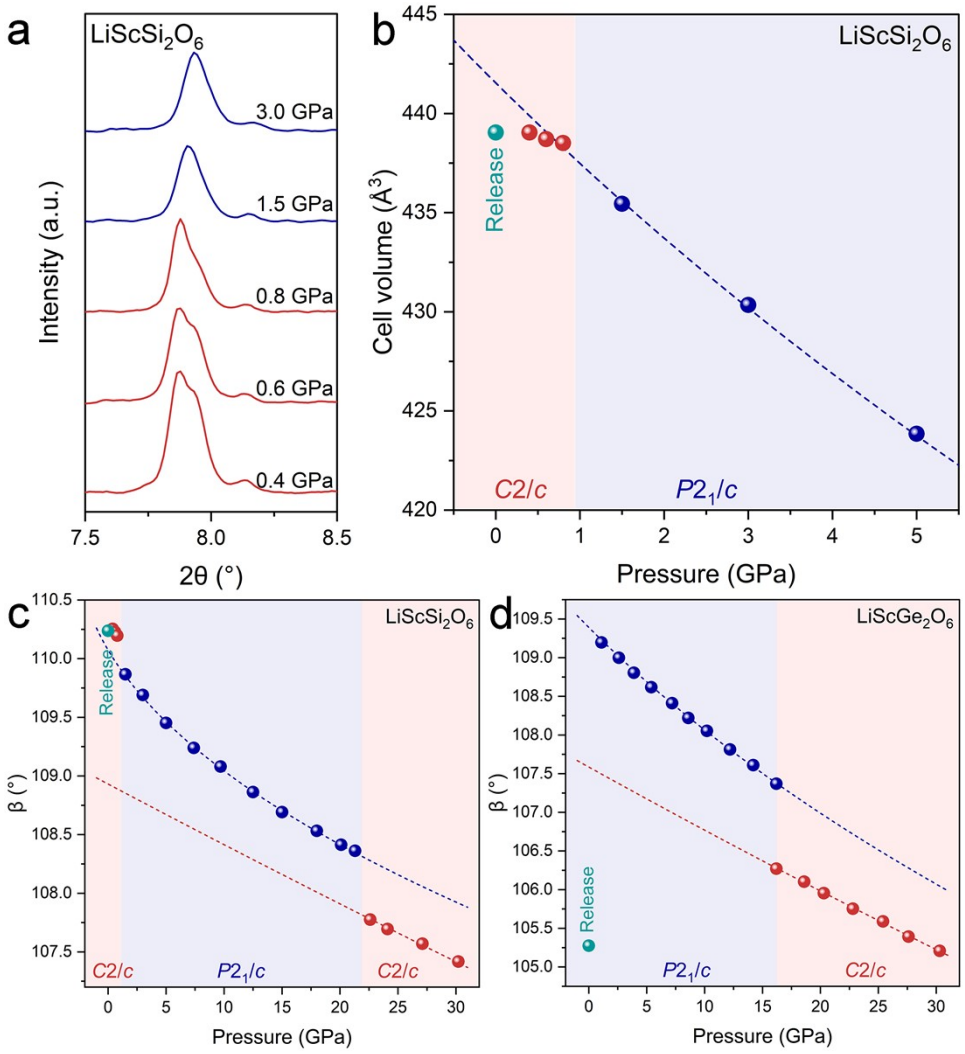

Figure S3. Partial enlargements of (a) *in situ* HP XRD pattern and (b) Lattice volume of $LiScSi_2O_6$. β angle of (c) $LiScSi_2O_6$ and (d) $LiScGe_2O_6$ as a function of pressure.

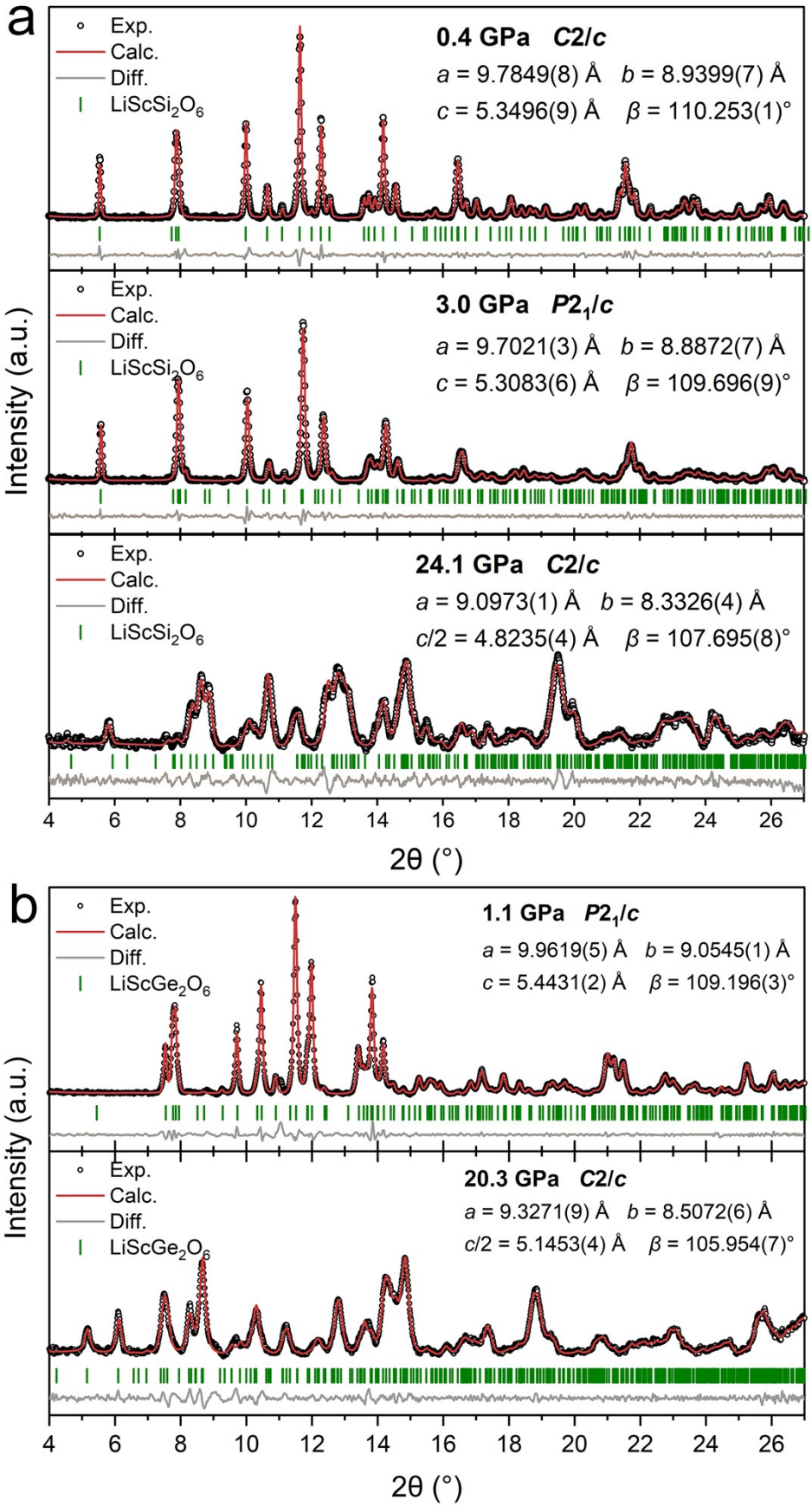

Figure S4. LeBail fitting results of (a) $LiScSi_2O_6$ at 0.4 GPa, 3.0 GPa, 24.1 GPa and (b) $LiScGe_2O_6$ at 1.1 GPa, 20.3 GPa.

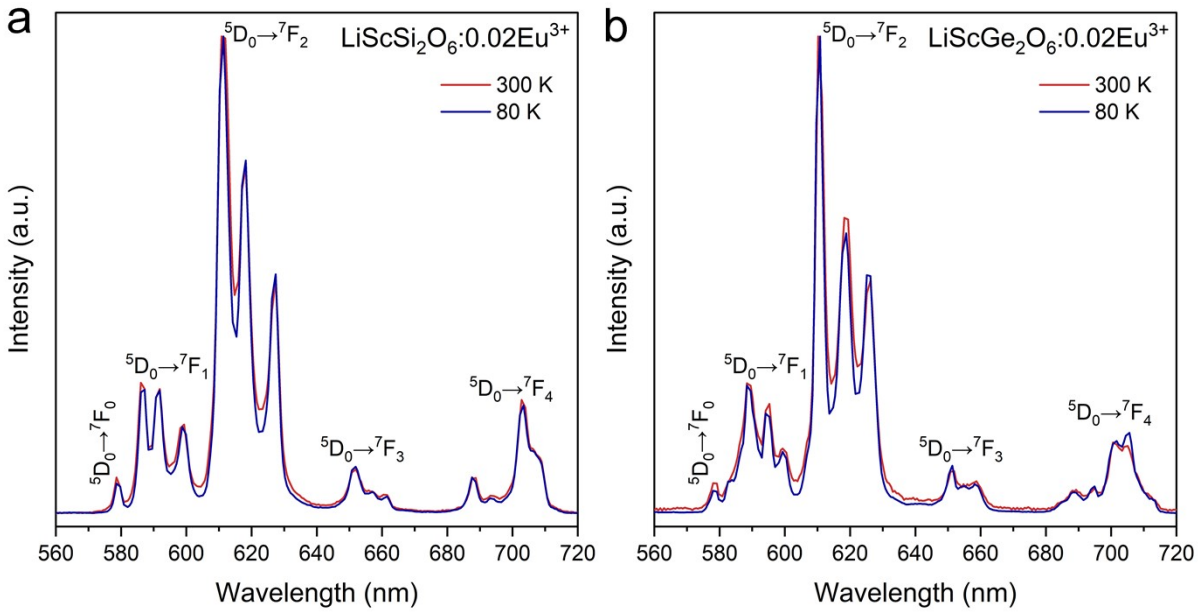

Figure S5. PL spectra of (a) $LiScSi_2O_6$:0.02Eu^{3+} and (b) $LiScGe_2O_6$:0.02Eu^{3+} measured at 80 K and 300 K.

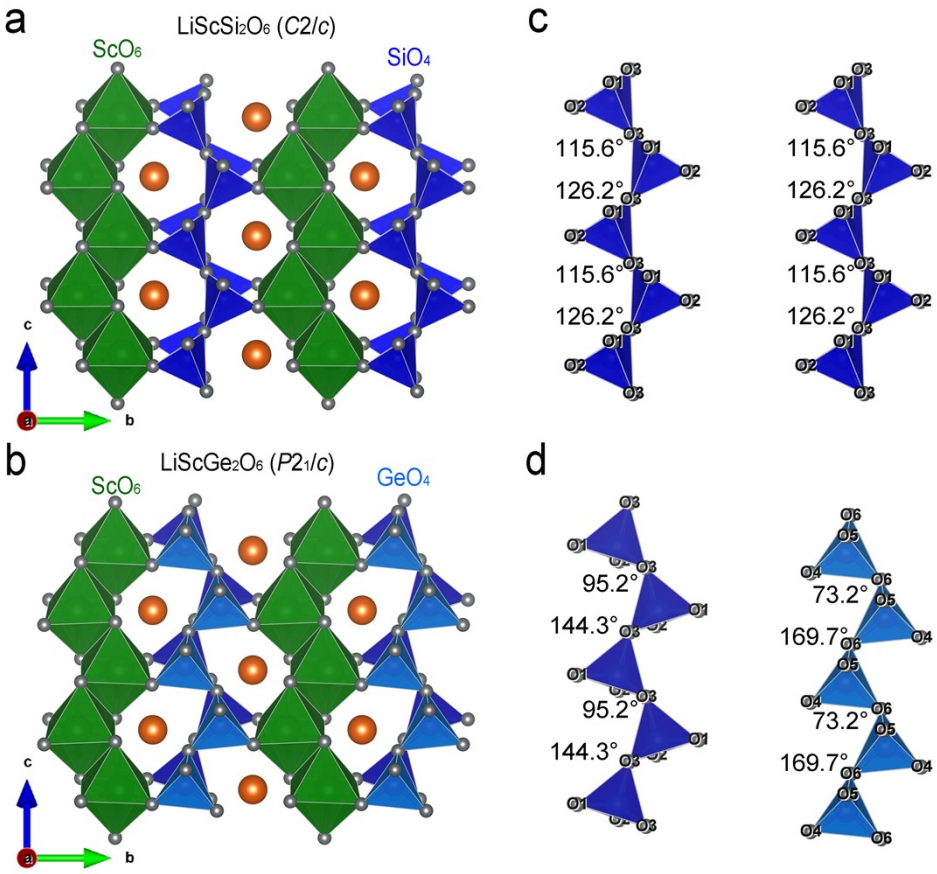

Figure S6. Crystal structures of (a) $LiScSi_2O_6$ and (b) $LiScGe_2O_6$. The twist angles of (c) SiO_4 tetrahedra chains in $LiScSi_2O_6$ and (d) GeO_4 tetrahedra chains in $LiScGe_2O_6$.

Table S1. Energy level transition and crystal field strength (D_q/B) of Some Cr^{3+} activated Phosphors at ambient conditions.

Materials	Cr sites	λ_{em} (nm)	Transition	D_q/B
$LiInGe_2O_6$:Cr	InO_6	880	$^4T_2 \rightarrow {}^4A_2$	1.66
$LiInSi_2O_6$:Cr	InO_6	840	$^4T_2 \rightarrow {}^4A_2$	1.75
$InBO_3$:Cr	InO_6	820	$^4T_2 \rightarrow {}^4A_2$	1.78
$LiScP_2O_7$:Cr	ScO_6	880	$^4T_2 \rightarrow {}^4A_2$	1.84
$LiScSi_2O_6$:Cr	ScO_6	850	$^4T_2 \rightarrow {}^4A_2$	1.87
$NaInGe_2O_6$:Cr	InO_6	900	$^4T_2 \rightarrow {}^4A_2$	1.89
$LiScGe_2O_6$:Cr	ScO_6	844-886	$^4T_2 \rightarrow {}^4A_2$	1.79-1.99
$Ca_2LuZr_2Al_3O_{12}$:Cr	CaO_8, LuO_8, ZrO_6	650-850	$^4T_2 \rightarrow {}^4A_2$	Cr1 1.92 Cr2 2.38
Sr_2ScSbO_6:Cr	ScO_6	890	$^4T_2 \rightarrow {}^4A_2$	2.03
$LiInP_2O_7$:Cr	InO_6	860	$^4T_2 \rightarrow {}^4A_2$	2.09
$CaMgGe_2O_6$:Cr	MgO_6	845	$^4T_2 \rightarrow {}^4A_2$	2.12
$ScBO_3$:Cr	ScO_6	800	$^4T_2 \rightarrow {}^4A_2$	2.15
$Sr_9Ga(PO_4)_7$:Cr	GaO_6	850	$^4T_2 \rightarrow {}^4A_2$	2.24
$GaTaO_4$:Cr	GaO_6	840	$^4T_2 \rightarrow {}^4A_2$	2.29
$Bi_2Ga_4O_9$:Cr	GaO_6	800	$^4T_2$, $^2E \rightarrow {}^4A_2$	2.31
$Ba_3Sc_4O_9$:Cr	ScO_6	835	$^4T_2 \rightarrow {}^4A_2$	Cr1 2.42 Cr2 2.40
$[EA]_2NaCr_xAl_{1-x}(HCOO)_6$	AlO_6	684.4, 686.4, 752.3	$^4T_2$, $^2E \rightarrow {}^4A_2$	2.76-2.33
La_2MgZrO_6:Cr	MgO_6, ZrO_6	740, 760, 825	^2E, $^4T_2 \rightarrow {}^4A_2$	2.53 2.49
Al_2O_3:Cr	AlO_6	694.28	$^2E \rightarrow {}^4A_2$	2.81
$LaGaO_3$:Cr	GaO_6	739	$^2E \rightarrow {}^4A_2$	2.89
$Zn_{2-x}Al_{2x}Sn_{1-x}O_4$:Cr	AlO_6	800-722	$^4T_2 \rightarrow {}^4A_2$	2.292-3.066
$BaAl_4Sb_2O_{12}$:Cr	AlO_6, SbO_6	695, 710, 750	$^2E \rightarrow {}^4A_2$	$[SbO_6]$2.6 $[AlO_6]$ 2.9
$Y_3Al_{5-x}Ga_xO_{12}$: Cr	AlO_6, GaO_6	688-691	$^2E \rightarrow {}^4A_2$	2.998-3.048